Impact of compatibility on the organization of mutualistic networks

Seong Eun Maeng,[1] Jae Woo Lee,[1,*] and Deok-Sun Lee[1,2,†]
[1]*Department of Physics, Inha University, Incheon 402-751, Korea*
[2]*Department of Natural Medical Sciences, Inha University, Incheon 402-751, Korea*
(Received 27 February 2013; revised manuscript received 5 July 2013; published 5 August 2013)

Distinct relationships such as activation, inhibition, cooperation, and competition are not established independently but in a correlated manner in complex systems. Thus the patterns of one type of interaction may reflect the impacts of other classes of interactions, but its quantitative understanding remains to be done. Referring to the plant-pollinator mutualistic networks, here we propose and investigate the structural features of a model bipartite network, in which the mutualistic relationship between two different types of nodes is established under the influence of the compatibility among the nodes of the same type. Interestingly, we find that the degree distributions obtained for extremely broad compatibility distributions are similar to those for a constant compatibility, both of which deviate from those for the Gaussian compatibility distributions. We present the analytic arguments to explain this finding. Also the dependence of the topological similarity of two nodes on their compatibility is illustrated. We discuss the application of our findings to complex systems.

DOI: 10.1103/PhysRevE.88.022804 PACS number(s): 89.75.Hc, 87.23.Kg, 05.40.−a

I. INTRODUCTION

Numerous species living in a region, individuals in a social group, and companies in an economic sector commonly form a variety of relationships among themselves to utilize limited resources and eventually flourish and prosper in a given system. The organizations of distinct classes of interactions can be captured by the network approach, which has been successful in unveiling the underlying design and working principles of complex systems [1]. The network structural characteristics may vary with the type of interaction as best seen in the ecological networks of predator-prey, host-parasite, plant-pollinator, anemone-fish, and so on [2,3]. For instance, the predator-prey networks display high modularity, as predators compete with one another, unwilling to share a prey [4]. On the contrary, the plant-pollinator mutualistic networks show high nestedness implying that pollinators tend to share plant species and also plants share pollinators [4,5].

Such distinct relationships can coexist in a given system, forming multiple layers of networks that are not independent [6,7]. Therefore much efforts have been made to identify layered structures and understand the effects of their interdependencies on the structure and function of diverse complex systems [8–12]. Nevertheless, the establishment and the interplay of those multiple layers of networks remain to be illuminated.

In an ecological community, insects get nutrients from plants during pollination and the plant species are reproduced by the pollination of animal species. The set of such mutualistic relationship among the species in a community can be represented by the mutualistic network and its topology and design principle have attracted much attention. To explain how the number of species, links, and the fraction of generalists and specialists are determined in the mutualistic networks, various computational models have been proposed and tested against the real-world data [13–22]. One of the main findings is that the species abundance and its asymmetry between plants and pollinators are supposed to be at work in designing the mutualistic networks [13,14]. It was also shown that the evolutionary duplication and divergence can be relevant factors, similarly to the evolution of protein-interaction networks [15]. A specific mutualistic pair of a plant and a pollinator is established depending on their biological matching, such as the proboscis length and the nectar depth [17,19]. Thus the model networks constructed depending on the biological matching between plants and pollinators have been investigated [16–22].

Recently we have shown that the preferential selection of partners can be the mechanism responsible for the observed topology of many mutualistic bipartite networks [23]. The functional form, linear or sublinear, of the preferential selection is shown to determine the asymptotic behaviors of the degree distribution, and we argued that the linear preferential selection can be changed to a sublinear one due to the competition between the same types of nodes. The competitive relationship between pollinators arises as the nutrients are provided by a limited number of plants, and similarly, the one between plants originates in a limited number of animals capable of pollinating plants.

In reality, the strength of competition can be varying from pair to pair. Moreover, a species may be neutral or favorable, not hostile, to another, in pollinating the same plant. If we use *compatibility* to denote the positive or negative relationship between the species of the same type, we can expect that two animal species with positive compatibility will pollinate the same plant species more likely than those with negative compatibility. We emphasize that the compatibility considered in this work is the one between the species of the same type, which should be distinguished from the biological matching between a plant and a pollinator considered in other previous works. The distribution of compatibility over node pairs thus can be a relevant factor to the organization of mutualistic relationship in a community. To address these issues quantitatively, we here propose and study a model bipartite network representing the mutualistic relationship between two distinct types of nodes, the evolution of which is affected by the compatibility

*jaewlee@inha.ac.kr
†deoksun.lee@inha.ac.kr

between nodes of the same type. It was proposed also in Ref. [21] that the relationship and the hierarchy of the animals foraging for resources provided by plants are the fundamental aspects of mutualistic networks as well as trophic ones. For the compatibility distributions displaying different asymptotic behaviors, we derive the connection probability of a node (plant) to a newly introduced node (pollinator) as a function of its degree and in turn the degree distributions, utilizing the similarity to the random-walk with variable step lengths or the so-called Lévy walk [24]. The degree distribution is found to take a power-law form when the compatibility is a positive constant for all pairs of nodes. In contrast, if the compatibility distribution is symmetric and broad, the degree distribution decays faster than a power law. However, interestingly, the deviation from a power-law form is less significant when the second moment of the compatibility distribution diverges than when it does not. We also examine the local connectivity pattern by computing the topological similarity (TS) between two nodes, defined as the number of their common partners. While the expected value of TS is negligible for large system sizes, it is shown to be of order 1 for large compatibility.

Our study illuminates the multiple relationships present in the ecological community. We consider two kinds of networks: One is the pollinator-pollinator compatibility network and the other is the plant-pollinator mutualistic network. To address this issue quantitatively, we focus on the impacts of the compatibility distribution on the topology of the mutualistic bipartite network. This paper is organized as follows. In Sec. II, we introduce the studied model network and describe the compatibility distributions considered in this work. The effective degree of a node and the degree distributions are derived and checked numerically with focus on their dependence on the functional form of the compatibility distribution in Sec. III. In Sec. IV, we obtain the TS between two nodes as a function of their compatibility and present their scaling properties. We summarize our findings and discuss their implications in Sec. V.

II. MODEL AND COMPATIBILITY DISTRIBUTIONS

Compatibilities among nodes are expected to play an important role in the organization of networked systems, which has been studied in the context of the evolution of unipartite networks [25]. In this section we introduce the compatibility-based growing bipartite network (CBGBN) model and the compatibility distributions to consider in this work.

Initially, there are ℓ_B nodes of type A and ℓ_A nodes of type B. Type A and B represent "animal" and "plant" in the plant-pollinator networks or two distinct types of nodes in general bipartite networks, e.g., "country" and "products" in the international-trade networks [23]. For the $\ell_A + \ell_B$ nodes at the initial stage, every pair of nodes of different types are connected. At each time step $\tau = 1,2,3,\ldots$, a new node τ of type A (B) is introduced with probability P_A (P_B), which is connected to ℓ_A (ℓ_B) preexisting nodes of type B (A). Here $P_A + P_B = 1$ and we index each node by its birth time. For the selection of partners, we first assign the compatibility value $x_{i\tau}$ to every node i of the same type as the new node τ, representing how compatible i and τ are. Then the effective degree $K_\ell(\tau)$ of each node ℓ of different type from τ is evaluated as

$$K_\ell(\tau) = \max\left\{0,\, x_{i_1\tau} + x_{i_2\tau} + \cdots + x_{i_{k_\ell}\tau}\right\}, \tag{1}$$

where $i_1, i_2, \ldots, i_{k_\ell}$ are the indices of the current partners of the node ℓ and k_ℓ is the degree of the node ℓ [Fig. 1(a)]. Note that if the sum of the compatibilities is negative, the effective degree is set to zero. A node ℓ is then selected with the probability

$$\frac{K_\ell(\tau)}{\sum_r{}' K_r(\tau)} \tag{2}$$

with $\sum'$ indicating the sum over the nodes of different type from the new node. Therefore two nodes having the same raw degree can have different selection probabilities depending on how compatible their current partners are with the new one. This selection is repeated ℓ_A times at every time step.

The compatibility x's are chosen independently from a given distribution $p(x)$. If the compatibility is a positive constant x_0 for every pair of nodes of one type, the effective degree K_ℓ of node ℓ of the other type is simply given by $x_0 k_\ell$ with k_ℓ the degree of ℓ. The corresponding compatibility distribution $p(x)$ takes a Dirac-delta function form

$$p^{(D)}(x) = \delta(x - x_0). \tag{3}$$

For the case of the compatibility values varying from pair to pair, we consider the Gaussian and the power-law distributions given by

$$p^{(G)}(x) = \frac{1}{\sqrt{2\pi}} e^{-x^2/2\sigma^2} \quad \text{for} \quad x \in (-\infty,\infty), \quad \text{and}$$
$$p^{(\alpha)}(x) = \begin{cases} \frac{\alpha}{2(\alpha+1)} x_0^{-1} & \text{for} \quad |x| < x_0, \\ \frac{\alpha}{2(\alpha+1)} \left|\frac{x}{x_0}\right|^{-\alpha-1} \frac{1}{x_0} & \text{for} \quad |x| > x_0, \end{cases} \tag{4}$$

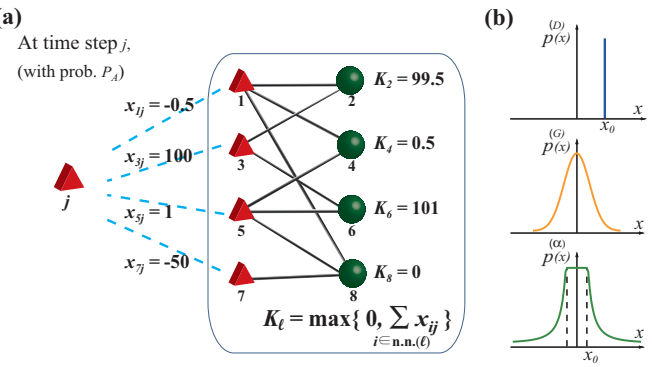

FIG. 1. (Color online) Compatibility-based growing bipartite network model. (a) Selection of partners of a new node. A new node j of type A (triangle) is introduced with probability P_A at a time step j in this example. The four preexisting type-A nodes are assigned x_{ij} ($i = 1,3,5$, and 7 in this example) representing their compatibility with the new node j. The effective degrees of type-B nodes ($\ell = 2,4,6,8$; circle) are then evaluated by Eq. (1). If the sum is negative, K_ℓ is set to zero. A node ℓ of type B is selected with the probability $\frac{K_\ell}{K_2+K_4+K_6+K_8}$, which is repeated ℓ_A times. (b) Schematic plots of the compatibility distributions considered in this work, the Dirac-delta function $p^{(D)}(x)$, the Gaussian function $p^{(G)}(x)$, and the power-law distribution $p^{(\alpha)}(x)$, from top to bottom. See Eqs. (3) and (4) for their definitions.

respectively, where σ and x_0 are constants and the exponent α is here set to be larger than 1. These distributions are symmetric, $p(-x) = p(x)$, and thus have zero mean $\overline{x} = \int dx\, x\, p(x) = 0$. However, they display different large-$|x|$ behaviors; the nth moment $\overline{x^n} = \int dx\, p(x)\, x^n$ is finite for every n with the Gaussian distribution, but it diverges for $n > \alpha$ with the power-law distributions. As seen in Fig. 1(b), the power-law distributions have fat tails compared with the Gaussian distributions, implying the larger likelihood to have extremely high or low compatibility with the power-law distributions.

For $p^{(G)}(x)$ or $p^{(\alpha)}(x)$, the compatibilities can be positive or negative. A preexisting node ℓ with many partners may have some of them compatible with the new node while others noncompatible or very hostile to the new node, thereby causing the effective degree of ℓ to be much smaller in magnitude than its raw degree k_ℓ. This is contrasted to the situation under a fixed compatibility, for which the effective degree is simply proportional to the raw degree.

We derive the effective degree in the case of the Gaussian and the power-law compatibility distribution in the next section, which enables us to see the impacts of heterogeneous compatibility distributions on the organization of the mutualistic relationship, as the mutualistic partners are determined based on the effective degrees. One can consider an asymmetric compatibility distribution, but the effective degree then becomes proportional to the raw degree on the average, which leads to the same results as for the case of the constant compatibility. Also, for simplicity, we set the compatibility between type-B nodes fixed at a positive constant and consider the three classes of compatibility distributions for type-A nodes. That is, only the compatibility between "animal" nodes are considered. The obtained results can be extended to the case of general compatibility distributions for both types of nodes.

III. EFFECTIVE DEGREE AND DEGREE DISTRIBUTIONS

In this section, we derive the effective degree of a type-B node determined by the compatibilities of its type-A partner nodes with the newly arrived node. Using the results for the effective degree, we next derive the degree distributions, for type-A and type-B nodes, respectively, in the CBGBN model. We begin with presenting the degree distributions obtained from the simulations of the model.

A. Degree distributions from simulation

In Fig. 2, the degree distributions of type-B nodes obtained from the simulation of the CBGBN model are presented for different compatibility distributions. When the compatibility is fixed, the degree distribution turns out to be a power law, implying the presence of many hub nodes of type B, originating in the selection probability proportional to the node degree as in the Barabási-Albert model for unipartite networks [26]. In contrast, for the Gaussian or the power-law compatibility distributions, the degree distributions are shown to have relatively fast-decaying tails, in a stretched-exponential form as will be shown below. This reflects the interference among the compatibilities, reducing the selection probability

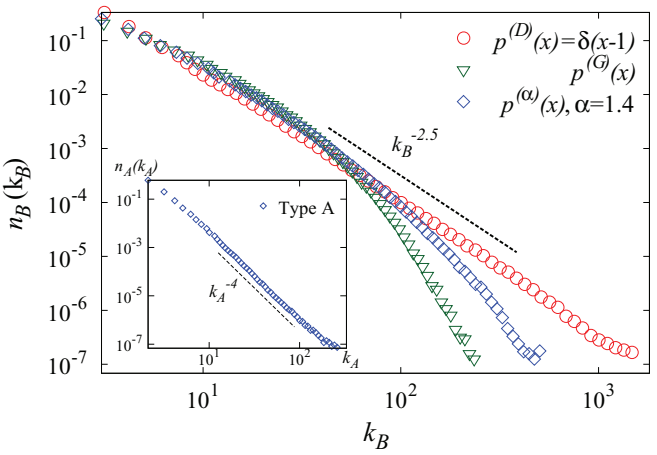

FIG. 2. (Color online) Degree distributions for the type-B nodes in the CBGBN model that evolves up to the final time step $\tau = 4 \times 10^4$ with $P_A = 0.75, P_B = 0.25, \ell_A = 2$, and $\ell_B = 3$. For the case of the constant compatibility 1 from $p^{(D)}(x) = \delta(x - 1)$, the degree distribution takes a power-law form $n_B(k_B) \sim k^{-\gamma_B}$ with $\gamma_B \simeq 2.4$ very close to 5/2 as predicted in Eqs. (27) and (29). The dashed line has slope -2.5. The degree distribution $n_B(k_B)$ for the Gaussian compatibility distribution deviates from the power-law form more significantly than that for the power-law compatibility distribution. Inset: Degree distribution for type-A nodes. It is a power law $n_A(k_A) \sim k_A^{-\gamma_A}$ with $\gamma \simeq 3.6$ close to 4 as given in Eqs. (28) and (29). The dashed line has slope -4.

of hub nodes that would be as high as proportional to their raw degrees without such heterogeneity of compatibility.

Given that the heterogeneity of compatibility leads the degree distributions to deviate from a power-law form, one would expect that the degree distribution decays faster for a power-law compatibility distribution than for a Gaussian one. However, Fig. 2 shows an unexpected result: The degree distribution for $p^{(\alpha)}(x)$ is closer to that for $p^{(D)}(x)$ than that for $p^{(G)}(x)$ is. To understand this result, we investigate analytically the effective degree and the degree distributions for each given compatibility distribution, which offers a quantitative way to understand the impacts of heterogeneous compatibility to the global organization of mutualistic networks.

B. Scaling of the expected effective degree

The probability for a node ℓ of type B to be selected as a mutualistic partner of the new node τ of type A is determined by its effective degree $K_\ell(\tau)$ in the CBGBN model. Recall that the effective degree of a type-A node is set to be equal to its raw degree. Given that the compatibility x's are independent each following a given compatibility distribution $p(x)$, $K_\ell(\tau)$ depends on the raw degree k_ℓ and the compatibility distribution $p(x)$. The average of the effective degree $\overline{K}_k$ of the nodes with degree k is evaluated as

$$\overline{K}_k = \int_0^\infty dy\, y P_k(y), \quad \text{with}$$
$$P_k(y) \equiv \int_{-\infty}^\infty dx_1\, p(x_1) \int_{-\infty}^\infty dx_2\, p(x_2) \cdots \int_{-\infty}^\infty dx_k\, p(x_k) \times \delta(x_1 + x_2 + \cdots + x_k - y). \quad (5)$$

Here we introduce the probability distribution $P_k(y)$ of the sum of k compatibility x's each commonly following $p(x)$. We explore the behavior of $P_k(y)$ to find out the functional behavior of $\overline{K}_k$.

We remark that the probability distribution $P_k(y)$ corresponds to the occupation probability of a random walker after k steps with the step length x following the same distribution as the compatibility distribution $p(x)$. $P_k(y)$ can take a non-Gaussian form if the step length is not always finite as in the Lévy walk [24].

If the compatibility takes a positive constant x_0 under the Dirac-delta-function-type compatibility distribution $p^{(D)}(x)$, it holds that

$$P_k^{(D)}(y) = \delta(y - k\,x_0), \tag{6}$$

leading the effective degree to be proportional to the degree k as

$$\overline{K}_k = k\,x_0. \tag{7}$$

To derive $P_k(y)$ for the Gaussian and the power-law compatibility distribution, let us consider the Fourier transforms $Q_k(s) = \int_{-\infty}^{\infty} dy\, P_k(y) e^{isy}$ and $q(k) = \int_{-\infty}^{\infty} dx\, p(x) e^{isx}$, which are related by $Q_k(s) = [q(s)]^k$. Once $Q_k(s)$ is known, one can derive $P_k(y)$ by the inverse Fourier transformation

$$P_k(y) = \frac{1}{2\pi} \int_{-\infty}^{\infty} ds\, Q_k(s) e^{-isy}. \tag{8}$$

For $p^{(G)}(x)$ in Eq. (4), its Fourier transform is of a Gaussian form as well,

$$q^{(G)}(s) = e^{-\sigma^2 s^2/2}, \tag{9}$$

and by using Eq. (8) we obtain

$$P_k^{(G)}(y) = \frac{1}{\sqrt{2\pi k \sigma^2}} e^{-y^2/2k\sigma^2}. \tag{10}$$

From Eq. (5), the effective degree is then given by

$$\overline{K}_k = \frac{\sigma}{2^{1/2}} k^{1/2}. \tag{11}$$

The effective degree for the Gaussian compatibility distribution is therefore much smaller than that for the constant compatibility in the regime $k \gg 1$, meaning that the hub type-B nodes are not so attractive to a new node as expected based on their large degrees. The exponent $1/2$ is characteristics of the Gaussian compatibility distribution and selected power-law ones as shown below.

The Fourier transform of the power-law compatibility distributions $p^{(\alpha)}(x)$ in Eq. (4) is expanded for $sx_0 \ll 1$ as

$$\begin{aligned} q^{(\alpha)}(s) &= \int_{-\infty}^{\infty} \frac{\alpha}{2(\alpha+1)} \min(|z|^{-\alpha-1}, 1) e^{i(sx_0)z} dz \\ &= \frac{\alpha}{\alpha+1} \frac{\sin sx_0}{sx_0} + \frac{\alpha}{\alpha+1} \int_1^{\infty} z^{-\alpha-1} \cos(sx_0 z) dz \\ &= 1 - \frac{\alpha}{6(\alpha-2)} (sx_0)^2 \\ &\quad + \frac{\alpha}{\alpha+1} \left(\cos\frac{\alpha\pi}{2} \right) \Gamma(-\alpha) (|s|x_0)^{\alpha} + \cdots, \end{aligned} \tag{12}$$

where $\Gamma(x)$ is the Gamma function and we used $\int_1^{\infty} dz\, z^{-\alpha-1} \cos(\beta z) = \beta^{\alpha} (\cos\frac{\alpha\pi}{2}) \Gamma(-\alpha) + \frac{1}{\alpha}\, {}_1F_2(-\frac{\alpha}{2}; \frac{1}{2}, 1 - \frac{\alpha}{2}; -\frac{\beta^2}{4})$ with the generalized hypergeometric function expanded as ${}_pF_q(a_1 \cdots a_p; b_1 \cdots b_q; Z) \simeq 1 + \frac{a_1 \cdots a_p}{b_1 \cdots b_q} Z + O(Z^2)$ for α not an integer. The quadratic term s^2 and the singular term s^{α} govern the small-s behavior of $q_{\alpha}(s)$ for $\alpha > 2$ and $1 < \alpha < 2$, respectively. We are concerned with the behaviors of $Q_k(s)$ and $P_k(y)$ for $k \gg 1$. If $\alpha > 2$, $Q_k(s)$ takes a Gaussian form

$$Q_k(s) \simeq e^{-(\sigma_{\alpha}^2/2) k s^2} \tag{13}$$

with $\sigma_{\alpha} = \sqrt{\frac{\alpha}{3(\alpha-2)}} x_0$. Note that $Q_k(s)$ is quite small for $s \gtrsim x_0^{-1}$ in the limit $k \to \infty$, making little contribution to the integral in Eq. (8) and thus justifying the use of Eq. (8) in the whole range of s. $Q_k(s)$ in Eq. (13) leads $P_k^{(2)}(y)$ to take the Gaussian form as in Eq. (10) with σ replaced by σ_{α}, and in turn, $\overline{K}_k$ is given by Eq. (11). On the other hand, for $1 < \alpha < 2$, it holds that

$$Q_k(s) \simeq e^{-\rho_{\alpha} k |s|^{\alpha}} \tag{14}$$

with $\rho_{\alpha} = \frac{\alpha}{\alpha+1} |\cos\frac{\alpha\pi}{2}| \Gamma(-\alpha) x_0^{\alpha}$. In this case, one can find that $P_k^{(\alpha)}(y)$ is expressed in terms of the scaling variable $y/k^{1/\alpha}$ as

$$P_k^{(\alpha)}(y) = \frac{1}{(\rho_{\alpha} k)^{1/\alpha}} \tilde{P}\left(\frac{y}{(\rho_{\alpha} k)^{1/\alpha}} \right), \tag{15}$$

where the scaling function $\tilde{P}(x)$ is defined as

$$\tilde{P}(x) = \frac{1}{\pi} \int_0^{\infty} \cos(xt)\, e^{-t^{\alpha}} dt \tag{16}$$

and behaves as

$$\tilde{P}(x) \simeq \begin{cases} \frac{\Gamma(1/\alpha)}{\pi\alpha} \exp\left[-\frac{\Gamma(3/\alpha)}{2\Gamma(1/\alpha)} x^2 \right] & \text{for} \quad x \ll 1, \\ \frac{\Gamma(\alpha+1)}{\pi} \sin\left(\frac{\pi\alpha}{2}\right) x^{-1-\alpha} & \text{for} \quad x \gg 1. \end{cases} \tag{17}$$

The derivation of Eq. (17) can be found in Refs. [27,28] and is also outlined in Appendix A. The scaling form of $P_k^{(\alpha)}(y)$ for $1 < \alpha < 2$ in Eq. (15) suggests that the effective degree scales with the raw degree as

$$\overline{K}_k = \int dy\, y P_k^{(\alpha)}(y) \simeq \kappa_{\alpha} k^{1/\alpha} \tag{18}$$

with κ_{α} a constant depending on α as $\kappa_{\alpha} = \rho_{\alpha}^{1/\alpha} \int_0^{\infty} dt\, t \tilde{P}(t)$.

We can summarize the above results for the effective degree as

$$\overline{K}_k \sim k^{\lambda}, \quad \lambda = \begin{cases} 1 & \text{for } p^{(D)}(x), \\ \frac{1}{2} & \text{for } p^{(G)}(x) \quad \text{or} \quad p^{(\alpha)}(x) \quad \text{with} \quad \alpha > 2, \\ \frac{1}{\alpha} & \text{for } p^{(\alpha)}(x) \quad \text{with} \quad 1 < \alpha < 2. \end{cases} \tag{19}$$

The nonlinear scaling of $\overline{K}_k$ with respect to k is found for heterogeneous compatibility distributions $p^{(G)}(x)$ and $p^{(\alpha)}(x)$ in our study. Since the selection probability of a node is proportional to its effective degree, our result implies that preexisting nodes with large degrees are not as often selected under the Gaussian compatibility distribution or the power-law

degree distribution as in the case of the fixed compatibility. A remarkable point is that such reduction of the selection probability of hub nodes is the most significant with the Gaussian compatibility distribution. For strongly broad compatibility distributions, the hub nodes recover their advantage in the partner selection. As the exponent α in the power-law compatibility distribution decreases, the scaling of the effective degree gets closer to the linear one; one can see in Eq. (19) that $\lambda \to 1$ as α decreases down to 2. We can attempt to understand this anomalous behavior as follows. When the compatibility is not fixed but distributed not so broadly, as for the Gaussian distribution or the power-law distribution with $\alpha > 2$, the positive and negative compatibility values of the k current partners in their relationship with the new node are comparable and likely to cancel each other, leading to $\overline{K}_k \sim k^{1/2}$ as in the conventional random walk. Note that in this case, the highest compatibility value X_k among k compatibilities behaves as $\sqrt{\ln k}$ or $k^{1/\alpha}$ ($\alpha > 2$) [29], and thus makes little contribution to the effective degree that turns out to behave as $\sqrt{k}$. In contrast, for such strongly broad compatibility distributions as $1 < \alpha < 2$, the extreme value makes a dominant contribution, as implied by the identical scaling behaviors of $X_k \sim k^{1/\alpha}$ and $\overline{K}_k \sim k^{1/\alpha}$. The destructive interference of the positive and negative compatibility values becomes irrelevant, recovering the advantage of hub nodes in the partner selection.

In Fig. 3, we numerically computed the ensemble average of $K_k = \max(0, x_1 + x_2 + \cdots + x_k)$ with k random numbers $x_1, x_2, \ldots, x_k$ generated from the distributions $P_D(x), P_G(x)$, or $P_\alpha(x)$, respectively. The obtained numerical results support Eq. (19). The deviation around $\alpha = 2$ may be rooted in the logarithmic correction $\overline{K}_k \sim \sqrt{k \ln k}$. For $\alpha = 2$, $q^{(2)}(s)$ is expanded for $sx_0 \ll 1$ as $q^{(2)}(s) \simeq 1 + \frac{1}{3}k(sx_0)^2 \ln|sx_0|$ yielding $Q_k(s) \simeq e^{(k/3)(sx_0)^2 \ln|sx_0|}$. As a result, $P_k^{(2)}(y)$ is represented in terms of the scaling variable $y/\sqrt{\frac{x_0^2}{6}k \ln k}$ as $P_k^{(2)}(y) = 1/\sqrt{\frac{x_0^2}{6}k \ln k}\,\tilde{P}(y/\sqrt{\frac{x_0^2}{6}k \ln k})$ and the effective degree scales as $\overline{K}_k \sim \sqrt{k \ln k}$. Thus the larger value of λ than $1/2$ observed in fitting $\overline{K}_k \sim k^\lambda$ to the simulation data may have been caused by the logarithmic correction term. More discussion on the logarithmic correction is given in Appendix B.

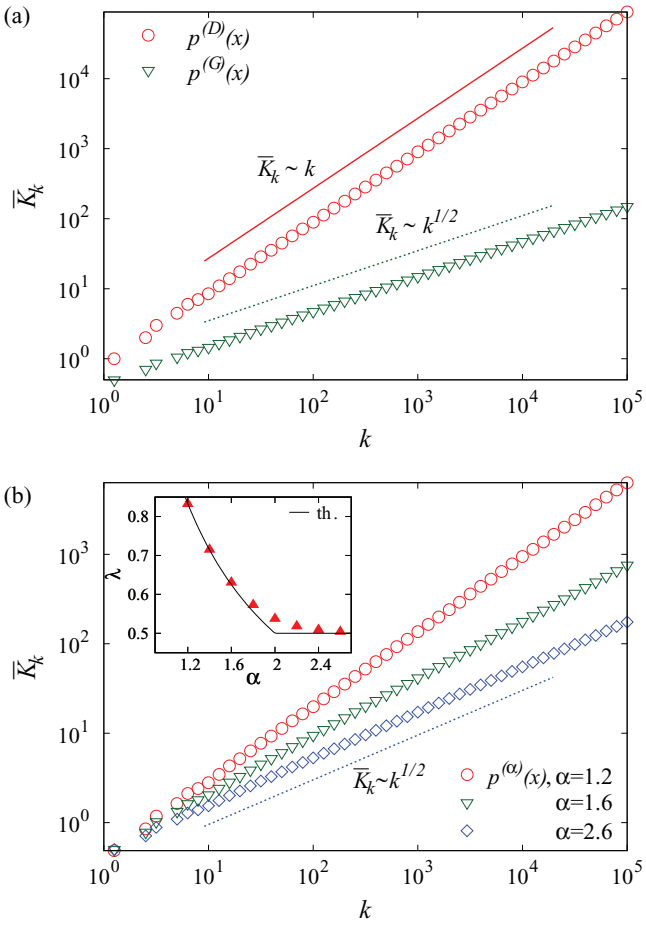

FIG. 3. (Color online) Scaling behaviors of the ensemble average $\overline{K}_k$ of $K_k = \max\{0, x_1 + x_2 + \cdots + x_k\}$ with x's independent random variables following a given distribution $p(x)$. (a) Plots of $\overline{K}_k$ versus k for the fixed compatibility $p^{(D)}(x) = \delta(x-1)$ and for the Gaussian compatibility distribution $p^{(G)}(x)$ with $\sigma = \sqrt{2\pi}$ chosen to yield the conditional average equal to 1; i.e., $\int_0^\infty dx\, x\, p^{(G)} / \int_0^\infty dx\, p^{(G)}(x) = 1$. The solid and dashed lines have slopes 1 and 1/2, respectively. (b) The same plots for the power-law compatibility distributions $p^{(\alpha)}(x)$. The dashed line has slope 1/2. Inset: The estimated exponent in the scaling relation $\overline{K}_k \sim k^\lambda$ as a function of α. The solid line indicates the theoretical prediction $\lambda = \max\{1/2, 1/\alpha\}$ given in Eq. (19).

C. Evolution and distribution of node degree

Using the results for the expected effective degree, we can investigate the evolution of node degrees and thereby derive the degree distributions. Nodes introduced at different time steps have different chances to attract new nodes, bringing broad degree distributions. We consider the averaged quantities over two types of stochasticity, one from the different realizations of the compatibility for each pair of nodes and the other from the selection of mutualistic partners given a realization of the compatibility relationship.

Let $a_{\ell\tau}$, taking 1 or 0, be the element of the adjacency matrix of the constructed network, denoting whether nodes ℓ and τ are connected or not. If two nodes ℓ and τ are of type B and A, respectively, and $\ell < \tau$, one can expect the corresponding element $\overline{a_{\ell\tau}^{(\mathrm{BA})}}$, averaged over different realizations of compatibility, to be given in terms of the effective degree of the node ℓ as

$$\overline{a_{\ell\tau}^{(\mathrm{BA})}} = f_{k_\ell}^{(\mathrm{BA})}(\tau) = \ell_A \frac{\overline{K}_{k_\ell}}{\sum_{r\in V_B} \overline{K}_{k_r}} \simeq \frac{k_\ell^\lambda}{\tau P_A \mu_B}, \tag{20}$$

where V_B is the set of nodes of type B at time step τ, and

$$\mu_B = \frac{1}{\tau P_A \ell_A} \sum_{r\in V_B} k_r{}^\lambda, \tag{21}$$

and we used Eq. (19) for the last approximation holding for k large. It should be noted that $0 \leqslant \overline{a_{\ell\tau}^{(\mathrm{BA})}} \leqslant 1$ and that $\sum_{\ell\in V_B} \overline{a_{\ell\tau}^{(\mathrm{BA})}} = \ell_A$. $f_k^{(BA)}(\tau)$ denotes the connection probability between a type-B node with degree k and a new type-A node at time step τ and is actually equal to $\overline{a_{\ell\tau}^{(\mathrm{BA})}}$. Similarly to Eq. (20), one finds that the probability that a node i of type A

and degree k_i is selected by a new node of type B at time step τ is given by

$$\overline{a_{i\tau}^{(\mathrm{AB})}} = f_{k_i}^{(\mathrm{AB})}(\tau) = \frac{k_i}{\tau P_B \mu_A} \tag{22}$$

with

$$\mu_A = \frac{1}{\tau P_B \ell_B} \sum_{j \in V_A} k_j = \frac{\langle \ell \rangle}{P_B \ell_B} = 1 + \frac{P_A \ell_A}{P_B \ell_B}, \tag{23}$$

and the number of links per node given by $\langle \ell \rangle = P_A \ell_A + P_B \ell_B$ [23].

The degree of a node increases by one if connected to a new node; hence its average degree evolves with time as

$$\begin{aligned} \left\langle k_\ell^{(\mathrm{B})}(\tau+1) \right\rangle - \left\langle k_\ell^{(\mathrm{B})}(\tau) \right\rangle &= P_A \left\langle \overline{a_{\ell\tau}^{(\mathrm{BA})}} \right\rangle + \ell_B \delta_{\ell,\tau}, \\ \left\langle k_i^{(\mathrm{A})}(\tau+1) \right\rangle - \left\langle k_i^{(\mathrm{A})}(\tau) \right\rangle &= P_B \left\langle \overline{a_{i\tau}^{(\mathrm{AB})}} \right\rangle + \ell_A \delta_{i,\tau}. \end{aligned} \tag{24}$$

Here $\langle Y \rangle$ indicates the average over different realizations of partner selection. In the limit $\tau \to \infty$, $\langle \overline{a_{i\tau}} \rangle$'s become quite small and thus one can approximate Eq. (24) as the differential equations $d\langle k_\ell^{(\mathrm{B})} \rangle / d\tau = P_A \langle \overline{a_{\ell\tau}^{(\mathrm{BA})}} \rangle = P_A \langle (k_\ell^{(\mathrm{B})})^\lambda \rangle / (\tau P_A \mu_B)$ and $d\langle k_i^{(\mathrm{A})} \rangle / d\tau = P_B \langle a_{i\tau}^{(\mathrm{AB})} \rangle = P_B \langle k_i^{(\mathrm{A})} \rangle / (\tau P_B \mu_A)$ with the initial condition $\langle k_\ell^{(\mathrm{B})}(\ell) \rangle = \ell_B$ and $\langle k_i^{(\mathrm{A})}(i) \rangle = \ell_A$. Solving these equations under the approximation $\langle (k_\ell^{(\mathrm{B})})^\lambda \rangle = \langle k_\ell^{(\mathrm{B})} \rangle^\lambda$ [30], one finds that the degree of a node increases with time as

$$\begin{aligned} \left\langle k_\ell^{(B)}(\tau) \right\rangle &= \ell_B \left[\frac{\ln\left(\eta \frac{\tau}{\ell}\right)}{\ln \eta} \right]^{\lambda/(1-\lambda)}, \\ \left\langle k_i^{(A)}(\tau) \right\rangle &= \ell_A \left(\frac{\tau}{i} \right)^{1/\mu_A}, \end{aligned} \tag{25}$$

where λ is given in Eq. (19) and $\ln \eta = \frac{\mu_B \ell_B^{1-\lambda}}{1-\lambda}$. The logarithmic dependence of k_ℓ on ℓ appears for the case of $\lambda < 1$, corresponding to the Gaussian and the power-law compatibility distributions.

The time evolution of the number of nodes of degree k and type B, $N_k^{(B)}(\tau) \equiv \sum_{\ell \in V_B} \langle \delta_{k_\ell,k} \rangle$, is also obtained in terms of the connection probability $f_k^{(\mathrm{BA})}(\tau)$ as

$$\begin{aligned} N_k^{(B)}(\tau+1) - N_k^{(B)}(\tau) = {} & P_B\, \delta_{k,\ell_B} + P_A\, f_{k-1}^{(\mathrm{BA})}(\tau)\, N_{k-1}^{(B)}(\tau) \\ & - P_A\, f_k^{(\mathrm{BA})}(\tau)\, N_k^{(B)}(\tau), \end{aligned} \tag{26}$$

and we find a similar equation for the degree distribution for type-A nodes. In the limit $\tau \to \infty$, the degree distributions defined by $n_B(k) = N_k^{(B)}(\tau)/(\tau P_B)$ and $n_A(k) = N_k^{(A)}(\tau)/(\tau P_A)$ become independent of time, and the recursive relations for them obtained by Eq. (26) lead to the following results [23]:

$$n_B(k) = \frac{\mu_B}{k^\lambda} \prod_{q=\ell_B}^{k} \frac{q^\lambda}{q^\lambda + \mu_B} \sim \begin{cases} k^{-\gamma_B} & \text{for } \lambda = 1, \\ \exp\left(-\mu_B \frac{k^{1-\lambda}}{1-\lambda}\right) & \text{for } \lambda < 1, \end{cases} \tag{27}$$

and

$$n_A(k) = \frac{\mu_A}{k} \prod_{q=\ell_A}^{k} \frac{q}{q + \mu_B} \sim k^{-\gamma_A}, \tag{28}$$

with

$$\gamma_A = 1 + \mu_A = 2 + \frac{P_A \ell_A}{P_B \ell_B}, \quad \gamma_B = 2 + \frac{P_B \ell_B}{P_A \ell_A}. \tag{29}$$

From Eqs. (19) and (27), one can see that the bipartite networks under the Gaussian and the power-law compatibility distribution for type-A nodes have $n_B(k)$ take a stretched-exponential form. In particular, $\ln n_B(k) \sim k^{1/2}$ universally for the Gaussian and the power-law compatibility distribution with $\alpha > 2$. This is contrasted to the power-law form of $n_B(k)$ in case of the constant compatibility. These results indicate that the heterogeneous compatibility makes a negative effect in the formation of hub nodes; the plant species (type B) with many pollinators do not attract as many pollinators as expected, owing to the negative compatibility (competition) between new pollinators and the current ones.

On the other hand, for the power-law compatibility distribution $p^{(\alpha)}(x)$ with $1 < \alpha < 2$, the bipartite network has more hub nodes as the compatibility distribution gets broader, i.e., α gets smaller. This phenomenon originates in the anomalous behavior of the effective degree discussed in Sec. III B; the extreme value among k compatibilities dominantly govern the behavior of the effective degree and increases faster with k as α decreases. Consequently, as α approaches 1, the functional form of the degree distribution $n_B(k)$ gets close to a power law, similar to the one obtained with the constant compatibility.

In Fig. 4, it is shown that the scaling behavior of the connection probability $f_k^{(\mathrm{BA})}(\tau)$ obtained numerically with respect to the raw degree k agrees well with the analytic results in Eq. (20). The power-law degree distribution emergent for the constant compatibility is replaced by the stretched-exponential one for the Gaussian and the power-law compatibility distribution [see Figs. 2 and 5(a)]. However, if we restrict ourselves to the latter case, we find that the broader the compatibility distribution is, the slower the degree distribution decays, getting closer to a power-law form, as shown in Fig. 5(b) and predicted in Eq. (27). While the finite-size effects are rather strong, the predicted stretched-exponential forms are supported by the simulation results in Fig. 5(b).

IV. TOPOLOGICAL SIMILARITY AND COMPATIBILITY

We have so far focused on the global organization of the mutualistic relationship. The influence of compatibility is, however, not restricted to the global characteristics but also identified in the local organization. In this section, we pay particular attention to the likelihood of sharing a common partner in the mutualistic network. The number of shared partners for a pair of nodes

$$k_{ij} = \sum_\ell a_{\ell i} a_{\ell j}, \tag{30}$$

with $a_{\ell j}$ the element of the adjacency matrix, is used to characterize their topological overlap [31]. In this work we call k_{ij} the topological similarity (TS) of two nodes i and j. The TS in Eq. (30) is used for measuring the nestedness of a network. Nestedness indicates the tendency that the set of the neighbor nodes of a node is included in that of another node having a larger degree [5]. A couple of measures of nestedness have been proposed [32] and one of the standard measures is

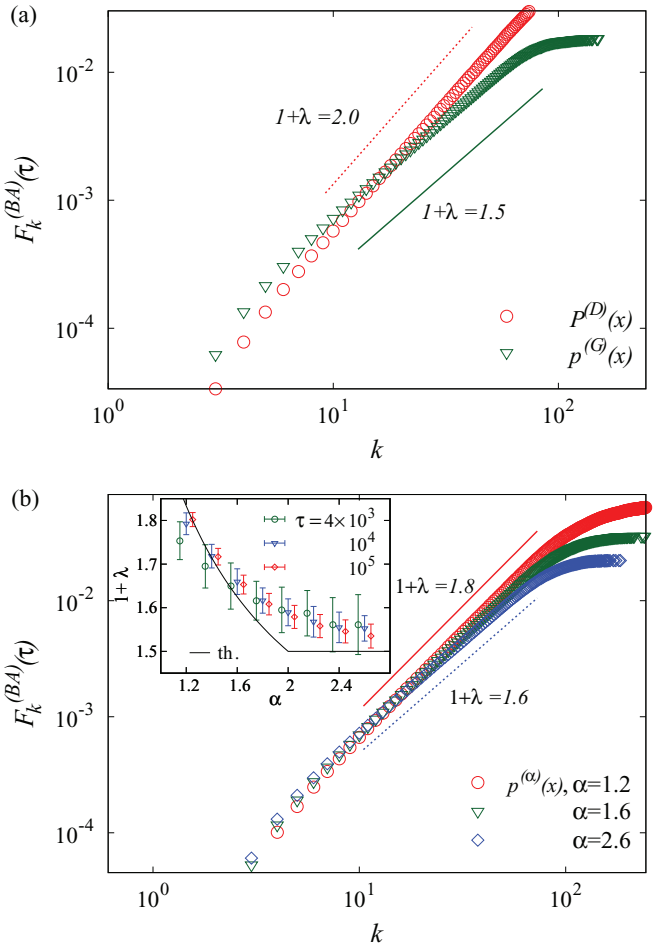

FIG. 4. (Color online) Cumulated connection probability $F_k^{(\mathrm{BA})}(\tau) = \sum_{k'=1}^{k} f_{k'}^{(\mathrm{BA})}(\tau)$ of a node of degree k and type B in the CBGBN model with $P_A = 0.75, P_B = 0.25, \ell_A = 2$, and $\ell_B = 3$ at the final time step (equal to the total number of nodes) $\tau = 4 \times 10^4$. (a) Plots of $F_k^{(\mathrm{BA})}(\tau)$ versus k for the constant compatibility $[p^{(D)}(x) = \delta(x-1)]$ and the Gaussian compatibility distribution $p^{(G)}(x)$ with $\sigma = \sqrt{2\pi}/2$. The scaling behaviors $F_k^{(\mathrm{BA})}(\tau) \sim k^{1+\lambda}$ are characterized by the scaling exponent $1+\lambda$ estimated to be 2.0 (dashed line) and 1.5 (solid line) for $p^{(D)}(x)$ and $p^{(G)}(x)$, respectively, in agreement with the analytic prediction from Eqs. (19) and (20). (b) The same plots for the power-law compatibility distributions $p^{(\alpha)}(x)$ with different exponents α. The estimated scaling exponents $1+\lambda$ decrease with α, from 1.8 (solid line) to 1.6 (dashed line). Inset: The estimated scaling exponent $1+\lambda$ as a function of α for different system sizes $\tau = 4 \times 10^3, 4 \times 10^4$, and 4×10^5. The solid line indicates the theoretical prediction $1+\lambda = 1 + \max\{1/2, 1/\alpha\}$ as given in Eq. (19). The deviation between the numerical results and the analytic result decreases as the system size τ increases.

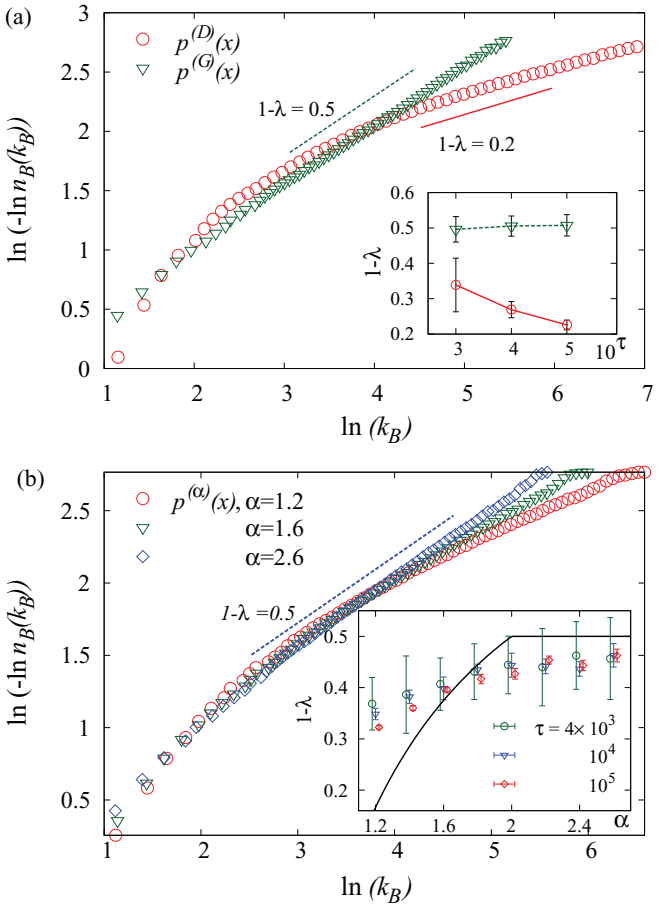

FIG. 5. (Color online) Asymptotic behaviors of the degree distribution $n_B(k)$ for type-B nodes in the CBGBN model. (a) Plots of $\ln[-\ln n_B(k_B)]$ versus $\ln k_B$ at the final time step $\tau = 4 \times 10^5$ for the constant compatibility $[p^{(D)}(x) = \delta(x-1)]$ and the Gaussian distribution $p^{(G)}(x)$ with $\sigma = \sqrt{2\pi}/2$. The slopes of these plots are estimated to be 0.5 (dashed line) and 0.2 (solid line), respectively, which can be compared with the analytic results from Eqs. (19) and (27). The smaller slope indicates the fatter tail of $n_B(k)$, here being the case for the constant compatibility. Inset: The estimated slopes, $1-\lambda$, as functions of the system size τ. The exponent is almost fixed at around 0.5 for the Gaussian compatibility distribution. On the other hand, the estimated slope $1-\lambda$ decreases with τ for the constant compatibility, implying the agreement with the analytic results $(1-\lambda = 0)$ in the limit $\tau \to \infty$. (b) The same plots for the power-law compatibility distributions with $\alpha = 1.2, 1.6$, and 2.6. The slope increases with α, indicating the fatter tail of $n_B(k)$ with the broader compatibility distributions. Inset: The estimated slopes, $1-\lambda$, as functions of α for different system sizes τ. As τ increases, the estimated values of $1-\lambda$ approach the analytic prediction (solid line) aside from the significant finite-size effects.

given by [33]

$$\eta = \frac{\sum_i \sum_{j>i} k_{ij}}{\sum_i \sum_{j>i} \min\{k_i, k_j\}}. \tag{31}$$

Therefore one can expect that the higher the TS between two nodes on the average is, the higher the nestedness of the whole network is. High nestedness is characteristic of the mutualistic networks [5] contrasted to the high modularity of the trophic networks [4]. Also the nestedness of the CBGBN model is larger than that of random networks, which is shown in detail in Appendix C.

In the CBGBN model, the TS, k_{ij}, depends not only on the degrees k_i and k_j but also on their compatibility, and in this section, we investigate how the mean TS between two nodes depends on their compatibility. Suppose that a node i of type A has compatibility x_{ij} with a new node j of type A at time step

$j(>i)$ and that a node ℓ of type B is already one of the partners of the older node i [see Fig. 1(a)]. Under this condition, one can expect the connection probability of ℓ to j should depend on the compatibility x_{ij}, the conditional probability of which we denote by $\langle f_{k_\ell}^{(BA)}\rangle_x$. Then the TS of two type-A nodes i and j having their compatibility x_{ij} is represented in terms of the conditional connection probability $\langle f_{k_\ell;x_{ij}}^{(BA)}\rangle$ of a node ℓ as

$$\begin{aligned}\left\langle k_{ij}^{(\mathrm{AA})}(\tau)\right\rangle_{x_{ij}} = P_B\Bigg[&\sum_{\ell=1}^{i-1}\left\langle f_{k_\ell}^{(BA)}(i)\right\rangle\left\langle f_{k_\ell}^{(BA)}(j)\right\rangle_{x_{ij}}\\ &+\sum_{\ell=i+1}^{j-1}\left\langle f_{k_i}^{(AB)}(\ell)\right\rangle\left\langle f_{k_\ell}^{(BA)}(j)\right\rangle_{x_{ij}}\\ &+\frac{\ell_B-1}{\ell_B}\sum_{\ell=j+1}^{\tau}\left\langle f_{k_i}^{(AB)}(\ell)\right\rangle\left\langle f_{k_j}^{(AB)}(\ell)\right\rangle\Bigg],\end{aligned}\tag{32}$$

where $\langle f_k^{(\mathrm{BA})}(\tau)\rangle$ and $\langle f_k^{(\mathrm{AB})}(\tau)\rangle$ can be evaluated by using Eqs. (20), (22), and (25). Notice that three summations in Eq. (32) distinguish the cases of $\ell<i<j, i<\ell<j$, and $i<j<\ell$, respectively. The factor $(\ell_B-1)/\ell_B$ was introduced to take into account that the number of ways for a new type-B node to select both i and j as its first ℓ_B partners is $\ell_B(\ell_B-1)$, not ℓ_B^2.

The probability $\langle f_{k_\ell}^{(BA)}(j)\rangle_{x_{ij}}$ for a node ℓ to be selected by node j is represented in terms of the conditional effective degree $\overline{K}_{k_\ell;x_{ij}}$ of the node ℓ as

$$f_{k_\ell;x_{ij}}^{(\mathrm{BA})}(j)=\ell_A\frac{\overline{K}_{k_\ell;x_{ij}}}{\sum_{r\in V_B}\overline{K}_{k_r}}\tag{33}$$

and $\overline{K}_{k_\ell;x_{ij}}$ can be obtained by using the probability distribution $P_k(y)$ studied in Sec. III B as

$$\begin{aligned}\overline{K}_{k_\ell;x_{ij}} &= \int_{-\infty}^{\infty}dx_1\,p(x_1)\cdots dx_{k_\ell-1}\,p(x_{k_\ell-1})\\ &\quad\times\max\{0,x_1+x_2+\cdots+x_{k-1}+x_{ij}\}\\ &=\int_{-\infty}^{\infty}dy\,P_{k_\ell-1}(y)\max\{0,y+x_{ij}\},\end{aligned}\tag{34}$$

where y indicates the sum of $k-1$ random variables following a given compatibility distribution $p(x)$.

While the exact functional form of $\overline{K}_{k_\ell;x_{ij}}$ can vary with the choice of the compatibility distribution, its limiting behaviors for $x_{ij}\gg 1$ and $x_{ij}\ll 1$ are robust against the variation of the compatibility distributions; the integral in Eq. (34) is dominantly contributed to by the integrand for small $|y|$, as all the compatibility distributions $p(x)$ decay faster than x^{-2}. In the case of $x_{ij}\ll -1$, one can see that $P_{k_\ell-1}(y)\max(y+x_{ij},0)\simeq 0$ for $|y|$ small and thus $\overline{K}_{k_\ell;x_{ij}}$ becomes negligible. For instance, see node "8" of type B in Fig. 1(a). This suggests that the node ℓ is hardly selected by the new node j owning to the bad relation between the partner node i of ℓ, and j. On the contrary, in the limit $x_{ij}\gg 1$, it holds that $P_{k_\ell-1}(y)\max(0,y+x_{ij})\simeq P_{k_\ell-1}(y)\,x_{ij}$ for $|y|$ small, leading to $\overline{K}_{k_\ell;x_{ij}}\simeq x_{ij}$. In other words, the extremely good compatibility between i and j dominates the effective degree of the node ℓ. See the nodes "2" or "6" in Fig. 1(a).

The asymptotic behaviors of $\overline{K}_{k_\ell;x_{ij}}$ are then summarized as

$$\overline{K}_{k_\ell;x_{ij}}\simeq\begin{cases}x_{ij} & \text{for}\quad x_{ij}\gg 1,\\ 0 & \text{for}\quad x_{ij}\ll -1.\end{cases}\tag{35}$$

From Eq. (35), we find that in the case of $x_{ij}\ll -1$, the connection probability is close to zero, $\langle f_{k_\ell}^{(\mathrm{BA})}(j)\rangle_{x_{ij}}\simeq 0$. In the case of $x_{ij}\gg 1$, the effective degree $\overline{K}_{k_\ell;x_{ij}}$ of the node ℓ is dominated by the compatibility x_{ij} between nodes i and j. Similarly, other partners of the node i have their effective degrees almost equal to x_{ij}. Therefore, if x_{ij} is extremely large, the sum of the effective degrees of all the type-B nodes appearing in the denominator in Eq. (33) will be approximated by $k_i(j)\,x_{ij}$, as the effective degrees of the nodes not connected to the node i are negligible. When x is not so large, the sum of the effective degrees does not explicitly depend on x but behaves as $\sum_{r\in V_B}\kappa_\alpha k_r(j)^\lambda\simeq\kappa_\alpha j P_A\mu_B$ with κ_α and μ_B given in Eqs. (18) and (21), respectively. Therefore the conditional connection probability $\langle f_{k_\ell}^{(\mathrm{BA})}\rangle_{x_{ij}}$ of the node ℓ is evaluated as

$$\left\langle f_{k_\ell;x_{ij}}^{(\mathrm{BA})}(j)\right\rangle\simeq\begin{cases}0 & \text{for}\quad x_{ij}\ll -1,\\ \frac{\tau_c x_{ij}}{j} & \text{for}\quad 1\ll x_{ij}\ll\frac{j}{\tau_c}\left(\frac{i}{j}\right)^{1/\mu_A},\\ \left(\frac{i}{j}\right)^{1/\mu_A} & \text{for}\quad x_{ij}\gg\frac{j}{\tau_c}\left(\frac{i}{j}\right)^{1/\mu_A},\end{cases}\tag{36}$$

where we used $\langle k_i^{(A)}(j)\rangle=\ell_A(j/i)^{1/\mu_A}$ in Eq. (25) for the node i of type A and a constant τ_c is defined as

$$\tau_c=\frac{1}{\kappa_\alpha P_A\mu_B}.\tag{37}$$

Using Eq. (36) in the first two summations in Eq. (32), we obtain the following behaviors of the TS of the nodes i and j at time step τ in the limit $\tau\to\infty$:

$$\left\langle k_{ij}^{(\mathrm{AA})}(\tau)\right\rangle_{x_{ij}}\simeq\begin{cases}b_{ij}(\tau) & \text{for}\quad x\ll -1,\\ \ell_A\frac{\tau_c x}{j}\left(\frac{j}{i}\right)^{\frac{1}{\mu_A}} & \text{for}\quad 1\ll x\ll\frac{j}{\tau_c}\left(\frac{i}{j}\right)^{\frac{1}{\mu_A}},\\ \ell_A & \text{for}\quad x\gg\frac{j}{\tau_c}\left(\frac{i}{j}\right)^{1/\mu_A},\end{cases}\tag{38}$$

where $b_{ij}(\tau)$ comes from the last summation in Eq. (32) with Eqs. (22) and (25) used and is evaluated as

$$\begin{aligned}b_{ij}(\tau)&\equiv P_B\frac{\ell_B-1}{\ell_B}\sum_{\ell=j+1}^{\tau}\left\langle f_{k_i}^{(\mathrm{AB})}(\ell)\right\rangle\left\langle f_{k_j}^{(\mathrm{AB})}(\ell)\right\rangle\\ &=P_B\frac{\ell_B-1}{\ell_B}\sum_{\ell=j+1}^{\tau}\ell_B\frac{\ell_A\left(\frac{\ell}{i}\right)^{\frac{1}{\mu_A}}}{\ell\langle\ell\rangle}\ell_B\frac{\ell_A\left(\frac{\ell}{j}\right)^{\frac{1}{\mu_A}}}{\ell\langle\ell\rangle}\\ &\simeq P_B\frac{\ell_B(\ell_B-1){\ell_A}^2}{\langle\ell\rangle^2}\left(\frac{1}{ij}\right)^{\frac{1}{\mu_A}}\frac{\tau^{\frac{2}{\mu_A}-1}-j^{\frac{2}{\mu_A}-1}}{\frac{2}{\mu_A}-1},\end{aligned}\tag{39}$$

and becomes a subdominant term in $\langle k_{ij}^{(\mathrm{AA})}(\tau)\rangle_{x_{ij}}$ for $x\gg 1$.

The results in Eq. (38) imply the following. When $x_{ij}\ll -1$, the TS of i and j can be generated only by the simultaneous selection by the type-B nodes that come later than them, the likelihood of which is $b_{ij}(\tau)$. As x_{ij} increases, j has the proportionately increasing chance to select the preexisting partners of i as one of its first ℓ_A partners and hence the linear behavior of $\langle k_{ij}^{(\mathrm{AA})}(\tau)\rangle_{x_{ij}}$ in x_{ij}. If x_{ij} is extremely large, j selects its first ℓ_A partners only among the partners of i; the

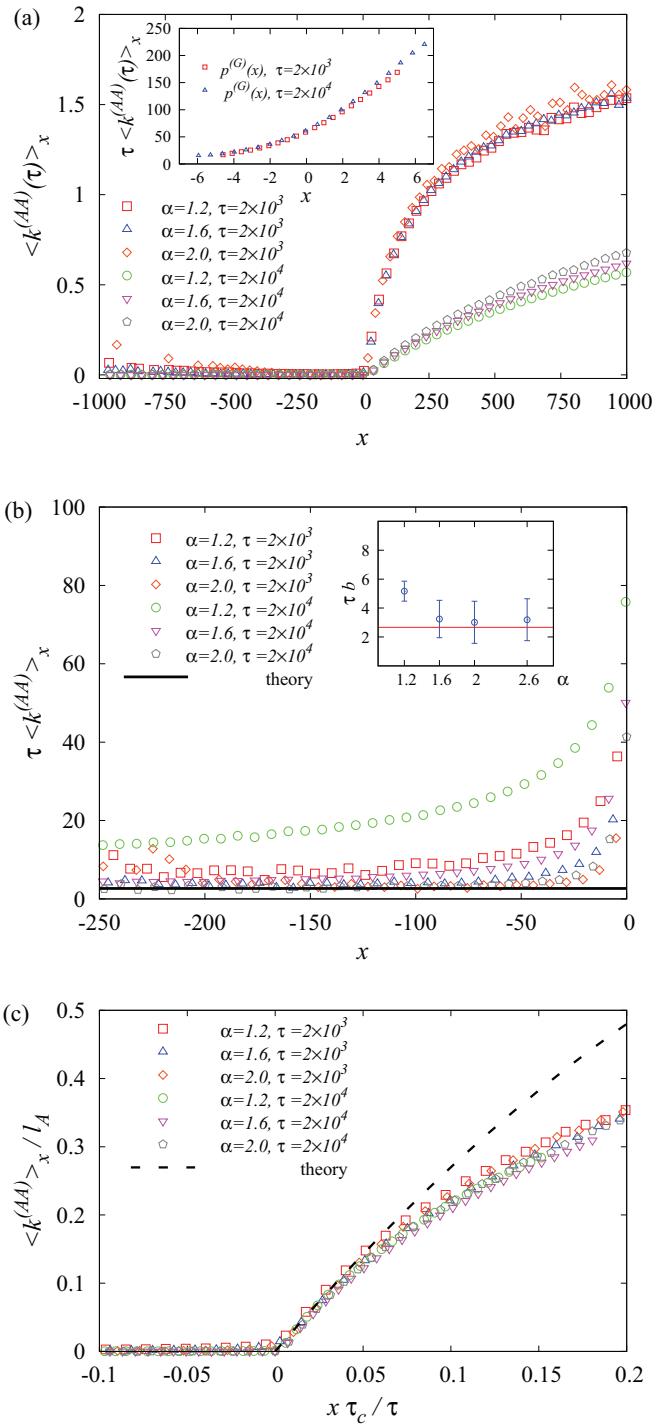

FIG. 6. (Color online) Numerical results for the mean TS $\langle k^{(\mathrm{AA})}(\tau)\rangle_x$ of the node pairs having compatibility x in the CBGBN model with $P_a = 0.75, P_B = 0.25, \ell_A = 2$, and $\ell_B = 3$. (a) Mean TS for the power-law compatibility distribution $p^{(\alpha)}(x)$ with different α's and different system size τ's. Inset: The plot of $\tau\langle k^{(\mathrm{AA})}(\tau)\rangle_x$ versus x for the Gaussian compatibility distributions. (b) Plots of $\tau\langle k^{(\mathrm{AA})}(\tau)\rangle_x$ versus x for $x < 0$ with the power-law compatibility distributions. As x decreases, the data points approach the theoretical prediction $\tau\, b = 8/3$ (dashed line) from Eq. (42). Inset: The fitting value of $\tau\, b$ for $\tau = 2 \times 10^4$ and different α's. (c) Plots of $\langle k^{(\mathrm{AA})}(\tau)\rangle_x$ versus $\tau_c\, x/\tau$ for different τ's and α's. The collapsed data agree with the theoretical prediction $\Phi(z) \simeq 2\mu_A z/(\mu_A - 1) - \mu_A z^2/(\mu_A - 2)$ from Eqs. (41) and (D7).

effective degrees of the partners of i are all given by x_{ij}, which are larger than those of any other nodes.

The TS for a randomly chosen pair of nodes having compatibility x, averaged over all possible pairs of nodes of type A, can be derived by using Eqs. (38) and (39) as

$$\langle k^{(\mathrm{AA})}(\tau)\rangle_x = \frac{2}{\tau^2}\sum_{i=1}^{\tau}\sum_{j=i+1}^{\tau}\left\langle k_{ij}^{(\mathrm{AA})}(\tau)\right\rangle_x = b(\tau) + \ell_A\,\Phi\left(\frac{\tau_c x}{\tau}\right), \tag{40}$$

where the scaling function $\Phi(z)$ behaves as

$$\Phi(z) \simeq \begin{cases} \frac{2\mu_A}{\mu_A - 1} z & \text{for} \quad z \ll 1, \\ 1 & \text{for} \quad z \gg 1, \end{cases} \tag{41}$$

and $b(\tau)$ is given by

$$b(\tau) = \frac{2}{\tau^2}\sum_{i=1}^{\tau}\sum_{j=i+1}^{\tau} b_{ij}(\tau) = \frac{P_B \ell_B(\ell_B - 1)}{P_A^2}\frac{1}{\tau}. \tag{42}$$

The derivation of the leading and subleading terms of the scaling function $\Phi(x)$ are given in Appendix D. In completely random bipartite networks of a total of τ nodes, the expected TS would be of order τ^{-1}. The TS in the CBGBN model, however, can be even of order 1 for a pair having very high compatibility, and the results in Eq. (40) show that the TS increases linearly for the moderately high compatibility.

The numerical results for the mean TS, $\langle k^{(\mathrm{AA})}(\tau)\rangle_x$, are presented in Fig. 6. The range of the observed compatibility values is wide for the power-law compatibility distributions but narrow for the Gaussian one. $\langle k^{(\mathrm{AA})}(\tau)\rangle_x$ remains negligible for $x < 0$, and increases with x for x positive, approaching its saturation value, ℓ_A in the limit $x \to \infty$, with the power-law compatibility distribution. The simulation results for the Gaussian compatibility distributions suggests $\langle k^{(\mathrm{AA})}(\tau)\rangle_x \sim \tau^{-1}$ in the observed range of x. In Fig. 6(b), the behavior of $\langle k^{(\mathrm{AA})}(\tau)\rangle_x$ for $x \ll -1$ with the power-law compatibility distributions is presented, which is in good agreement with the prediction in Eq. (42) even for coefficient. Rescaling x by τ_c/τ for x positive as suggested in Eq. (40), we obtain the predicted collapse of $\langle k^{(\mathrm{AA})}(\tau)\rangle_x$ from different τ's and α's in Fig. 6(c). The parameter τ_c depends on α via κ_α and μ_B, which are obtained numerically for the plots in Fig. 6(c). Furthermore, the collapse data confirm the predicted behavior of the scaling function $\Phi(z)$ in Eq. (41).

V. SUMMARY AND DISCUSSION

The specific mutualistic pairs of plants and pollinators in an ecological community can be fully understood by considering diverse factors such as the species abundance, biological matching, and evolutionary processes. However, many studies commonly suggest that a few simple mechanisms are sufficient to understand the selected topological features of the mutualistic networks. We have shown in our previous work [23] that the growing bipartite networks with preferential attachment can successfully reproduce the global properties of many real-world plant-pollinator mutualistic networks. However, it remained poorly understood how the functional form of the preferential attachment is determined.

In this work, we proposed and investigated the growing bipartite network model representing the evolution of the mutualistic relationship between two distinct groups of species that are influenced by the compatibility within the same groups. Our results illuminate the multiplex nature of mutualistic communities; every species belongs to the compatibility network, in which each link connecting the same types of species (animal-animal or plant-plant) is assigned weight equal to their compatibility, and also belongs to the mutualistic network. We demonstrated the impacts of the link weight distribution in one (compatibility) network to the topology of the other (mutualistic) network.

The effective degree of a node determined by the compatibility of its current partners governs the evolution dynamics and thereby the architecture of the mutualistic network. The effective degree was derived for each given compatibility distribution and the results show how the form of the preferential attachment can be changed depending on the compatibility distribution. Furthermore, using the results, we obtained the degree distributions and the topological similarity conditioned on the compatibility.

All these results demonstrate the crucial impacts of the compatibility on the network structure of the mutualistic relationship. The degree distribution takes a faster-decaying tail than a power law, preventing the appearance of hub nodes, as long as the compatibility value varies from pair to pair. However, as the compatibility distribution gets broader, the degree distributions go back towards the power-law form that appears for the case of the constant compatibility. Also, we showed how the topological similarity between two nodes can be varied depending on their compatibility, which can be one of the mechanisms driving the heterogeneity of the topological similarity, more significant than the random expectation, in various complex networks. While our model reproduces successfully the degree distributions of mutualistic networks and offer insights into the topological similarity, it may need to be improved and extended to reproduce many other properties such as modularity and nestedness of real mutualistic networks.

While we focused on the specific types of interactions that are present in the mutualistic community, our results can be applied to the analysis of other types of interactions in diverse complex systems. Our work proves the importance of considering the interaction among different types of interactions in the evolution, structure, and dynamics of complex systems and thus can contribute to establishing the theoretical framework to analyze various complex systems.

ACKNOWLEDGMENTS

This work was supported by Basic Science Research Program through the National Research Foundation of Korea (NRF) funded by the Ministry of Education, Science, and Technology [Grants No. 2012R1A1B3001183 (J.W.L) and No. 2012R1A1A2005252 (D.-S.L)]. Numerical computations were supported by the National Institute of Supercomputing and Networking/Korea Institute of Science and Technology Information with supercomputing resources including technical support (KSC-2012-C1-18).

APPENDIX A: DERIVATION OF EQ. (17)

Here we outline the derivation of Eq. (17) given in Refs. [27,28]. The expansion of the function $\tilde{P}(x)$ in Eq. (16) for $x \ll 1$ can be obtained by using the expansion $\cos(xt) = \sum_{n=0}^{\infty} t^{2n}(-x^2)^n/(2n)!$ as

$$\begin{aligned}\tilde{P}(x) &= \frac{1}{\pi}\sum_{n=0}^{\infty}\frac{(-1)^n}{(2n)!}x^{2n}\int_0^{\infty} dt\, t^{2n}e^{-t^{\alpha}} \\ &= \frac{1}{\pi\alpha}\sum_{n=0}^{\infty}\frac{(-1)^n\Gamma\left(\frac{2n+1}{\alpha}\right)}{(2n)!}x^{2n} \\ &\simeq \frac{\Gamma(1/\alpha)}{\pi\alpha}\left[1-\frac{1}{2}\frac{\Gamma(3/\alpha)}{\Gamma(1/\alpha)}x^2\right], \end{aligned} \tag{A1}$$

where we used $\Gamma(z) = \int_0^{\infty} t^{z-1}e^{-t}dt$. The large-$x$ behavior of $\tilde{P}(x)$ can be seen by expanding $e^{-t^{\alpha}}$ and using $\int_0^{\infty} dt\, t^{z-1}e^{i\omega t} = \omega^{-z}\Gamma(z)e^{iz\pi/2}$ as

$$\begin{aligned}\tilde{P}(x) &= \frac{1}{\pi}\sum_{n=0}^{\infty}\frac{(-1)^n}{n!}\int_0^{\infty} dt\, t^{\alpha n}\cos(xt) \\ &= \frac{1}{\pi}\sum_{n=0}^{\infty}\frac{(-1)^{n+1}}{n!}\Gamma(\alpha n+1)\sin\left(\frac{\alpha n}{2}\pi\right)x^{-1-\alpha n} \\ &\simeq \frac{\Gamma(\alpha+1)}{\pi}\sin\left(\frac{\pi\alpha}{2}\right)x^{-1-\alpha}. \end{aligned} \tag{A2}$$

APPENDIX B: LOGARITHMIC CORRECTION TO THE EFFECTIVE DEGREE IN THE CASE OF $\alpha = 2$

If $\alpha = 2$ in Eq. (4), the compatibility distribution shows the asymptotic behavior $p(x) \sim |x|^{-3}$ and consequently, the effective degree scales as $\overline{K}_k \sim \sqrt{k\ln k}$, not $k^{1/2}$. Here we briefly explain how such a logarithmic correction appears.

The integral $\int_1^{\infty} z^{-3}\cos(\beta z)$ appearing in Eq. (12) is expanded for small β as

$$\begin{aligned}\int_1^{\infty} z^{-3}\cos(\beta z) &= \frac{1}{2}\cos\beta + \frac{\beta^2}{2}Ci(\beta) - \frac{\beta^3}{2}\sin\beta, \\ Ci(\beta) &= \int_{\infty}^{\beta} t^{-1}\cos t\, dt \\ &= \gamma + \ln\beta + \sum_{k=1}^{\infty}\frac{(-\beta^2)^k}{2k(2k)!}, \end{aligned} \tag{B1}$$

where γ is the Euler-Mascheroni constant. Therefore $q^{(2)}(s)$ is expanded for small sx_0 as

$$q^{(2)}(s) \simeq 1 + \tfrac{1}{3}(sx_0)^2\ln|sx_0| \tag{B2}$$

and $Q_k(s) = [q^{(2)}(s)]^k$ is given by

$$Q_k(s) \simeq e^{(k/3)(sx_0)^2\ln|sx_0|}. \tag{B3}$$

This expression is valid for $sx_0 \ll 1$. Using Eq. (B3) in place of $Q_k(s)$ of Eq. (8), we find two characteristic scales of s, y^{-1} and $1/\sqrt{\frac{x_0^2}{6}k\ln k}$, and the function $P_k^{(2)}(y)$ is represented in

terms of their ratio as the scaling variable as

$$P_k^{(2)}(y) = \frac{1}{\sqrt{\frac{x_0^2}{6}k\ln k}}\tilde{P}\left(\frac{y}{\sqrt{\frac{x_0^2}{6}k\ln k}}\right). \tag{B4}$$

Therefore the effective degree is given the additional logarithmic term as $\overline{K}_k = \int dy\, y P_k^{(2)}(y) \simeq \kappa_2\sqrt{k\ln k}$ with $\kappa_2 = (x_0/\sqrt{6})\int_0^\infty dt\, t\tilde{P}(t)$. The small-$x$ and large-x behaviors of the scaling function $\tilde{P}(x)$ can be obtained as follows.

For $y \ll x_0\sqrt{k\ln k}$, we use the expansion $\cos(ys) = \sum_{n=0}^\infty \frac{(-1)^n}{(2n)!}y^{2n}s^{2n}$ to represent $P_k^{(2)}(y)$ as

$$P_k^{(2)}(y) = \sum_{n=0}^\infty \frac{(-1)^n}{(2n)!}y^{2n}\frac{1}{\pi}\int_0^\infty ds s^{2n}Q_k(s) \tag{B5}$$

with $Q_k(s)$ in Eq. (B3). Using the steepest-descent method, one finds that the integral $I_m(\kappa) \equiv \int_0^\infty t^{m-1}e^{\kappa t^2\ln t}$ is dominantly contributed to by the integrand at $t_* = [(m-1)/(\kappa\ln\kappa)]^{1/2}$ for κ large and is therefore approximated by

$$I_m(\kappa) \simeq \frac{\pi^{1/2}e^{-(m-1)/2}(m-1)^{(m-1)/2}}{(\kappa\ln\kappa)^{m/2}}. \tag{B6}$$

Inserting Eq. (B6) into Eq. (B5) with $\kappa = k/3$ and $m = 2n+1$, we find that

$$\begin{aligned} P_k^{(2)}(y) &\simeq \left(\frac{3}{\pi x_0^2 k\ln k}\right)^{1/2}\sum_{n=0}^\infty \frac{(-1)^n}{(2n)!}\left(\frac{6ne^{-1}y^2}{x_0^2 k\ln k}\right)^n \\ &\simeq \left(\frac{3}{\pi x_0^2 k\ln k}\right)^{1/2}\left[1-\frac{3e^{-1}y^2}{x_0^2 k\ln k}\right], \end{aligned} \tag{B7}$$

where the last approximation holds for $y \ll x_0\sqrt{k\ln k}$. Therefore we find that the scaling function $\tilde{P}(x)$ in Eq. (B4) behaves as $(2\pi)^{-1/2}e^{-e^{-1}x^2/2}$ for $x \ll 1$.

For $y \gg x_0\sqrt{k\ln k}$, we perform the partial integration to obtain

$$\begin{aligned} P_k^{(2)}(y) &= -\frac{1}{\pi}\int_0^\infty ds\frac{\sin(ys)}{y}\frac{dQ_k(s)}{ds} \\ &\simeq -\frac{1}{\pi}\int_0^\infty d(sx_0)\frac{\sin(ys)}{y}\frac{2k}{3}(sx_0)\ln(sx_0)\,Q_k(s). \end{aligned} \tag{B8}$$

The dominant contribution to the integral in Eq. (B8) comes from the range $0 \leqslant s \lesssim y^{-1}$ given the exponential decay of $Q_k(s)$ and the oscillatory behavior of $\sin(ys)$. Using $Q_k(s) \simeq 1$ for $0 \leqslant s \lesssim y^{-1}$, we obtain the following approximate expression for $P_k^{(2)}(y)$:

$$\begin{aligned} P_k^{(2)}(y) &\sim -\frac{2kx_0^2}{3\pi y^3}\int_0^1 dz\, z\sin z\ln\left(z\frac{x_0}{y}\right) \\ &\sim \frac{kx_0^2\ln y}{y^3}. \end{aligned} \tag{B9}$$

Therefore we find that the scaling function $\tilde{P}(x)$ behaves as $\tilde{P}(x) \sim x^{-3}$ for $x \gg 1$.

APPENDIX C: NESTEDNESS OF THE CBGBN MODEL

Extending the measure of nestedness in Eq. (31) to bipartite networks, we can define the nestedness of the nodes of type A in a bipartite network as

$$\eta^{(\mathrm{A})} = \frac{\sum_{i\in V_A}\sum_{j\in V_A, j>i}k_{ij}^{(\mathrm{AA})}}{\sum_{i\in V_A}\sum_{j\in V_A, j>i}\min\left\{k_i^{(\mathrm{A})},k_j^{(\mathrm{A})}\right\}}, \tag{C1}$$

where $k_i^{(A)}$ is the degree of a node of type A and $k_{ij}^{(\mathrm{AA})}$ is the number of common partners (neighbor nodes) of two nodes i and j both of type A. Similarly, we can define $\eta^{(\mathrm{B})}$.

Using Eq. (C1), we obtained numerically the nestedness of the CBGBN model and compared it with that of the random networks. Random networks were constructed by assigning links to a randomly chosen pair of nodes with the number of nodes and the number of links identical to those of the considered model networks. As in the main text, we considered various compatibility distributions for type-A nodes and the fixed compatibility for type-B nodes. The results are given in Fig. 7, in which the nestedness for nodes of type A and B are given as a function of the number of nodes N.

The nestedness in the CBGBN model is much higher than in the random networks. In the model networks, hub plant (type-B) nodes are more likely to be connected to a new animal (type-A) node, as their selection probability is higher than the plants with few partners given that the selection probability of a plant node scales linearly or sublinearly with its raw degree. The animal species are therefore more likely to be the partners of a hub plant species, and thus the hub plant node tends to be the common partner of many animal species. Abundant hub plant nodes in the CBGBN model therefore lead to the enhancement of $k_{ij}^{(\mathrm{AA})}$ on the average and the enhancement of the nestedness of animal nodes. The same holds for $k_{ij}^{(\mathrm{BB})}$ and $\eta^{(B)}$.

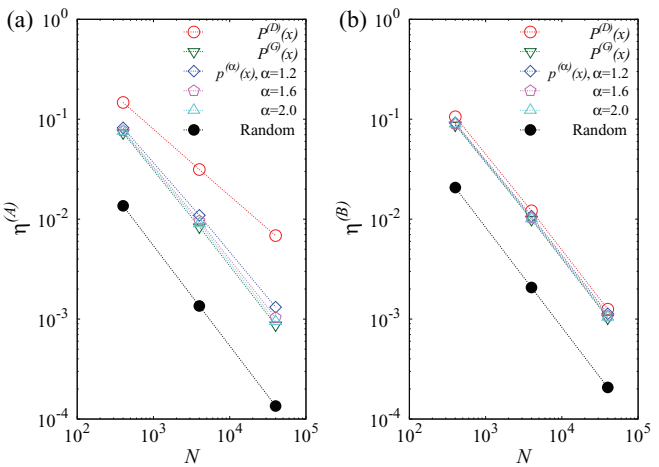

FIG. 7. (Color online) Comparison of the nestedness η between the CBGBN model and random bipartite networks. (a) Plots of $\eta^{(\mathrm{A})}$ versus the total number of nodes N for selected compatibility distributions. Here the model parameters are $P_A = 0.75, P_B = 0.25, \ell_A = 2$, and $\ell_B = 3$. The random bipartite networks have the same number of nodes of type A and B and the same number of links as the CBGBN model. (b) Plots of $\eta^{(\mathrm{B})}$ for the CBGBN model and the random bipartite networks.

APPENDIX D: DERIVATION OF EQS. (40), (41), AND (42)

The coefficient $b(\tau)$ in Eq. (42) is obtained by using Eq. (39) in the limit $\tau \to \infty$ as

$$\begin{aligned} b(\tau) &\simeq \frac{2P_B\ell_B(\ell_B-1)\ell_A^2}{\tau^2\langle\ell\rangle^2\left(\frac{2}{\mu_A}-1\right)}\sum_{i=1}^{\tau}\frac{1}{i^{\frac{1}{\mu_A}}} \\ &\quad\times\left[\tau^{\frac{2}{\mu_A}-1}\left\{\frac{\tau^{1-\frac{1}{\mu_A}}-i^{1-\frac{1}{\mu_A}}}{1-\frac{1}{\mu_A}}\right\}-\left\{\frac{\tau^{\frac{1}{\mu_A}}-i^{\frac{1}{\mu_A}}}{\frac{1}{\mu_A}}\right\}\right] \\ &\simeq \frac{2P_B\ell_B(\ell_B-1)\ell_A^2}{\tau^2\langle\ell\rangle^2\left(\frac{2}{\mu_A}-1\right)}\left[\frac{\mu_A(2-\mu_A)\tau^{\frac{1}{\mu_A}}}{\mu_A-1}\frac{\tau^{1-\frac{1}{\mu_A}}-1}{1-\frac{1}{\mu_A}}\right. \\ &\quad\left.-\frac{\mu_A\tau^{\frac{2}{\mu_A}-1}}{\mu_A-1}\frac{\tau^{2-\frac{2}{\mu_A}}-1}{2-\frac{2}{\mu_A}}+\mu_A(\tau-1)\right] \\ &\simeq \frac{\ell_A^2(\ell_B-1)}{\langle\ell\rangle}\frac{\mu_A}{(\mu_A-1)^2}\frac{1}{\tau}. \end{aligned} \tag{D1}$$

The function Φ in Eq. (41) represents the x dependence of $\langle k^{(\mathrm{AA})}(\tau)\rangle_x$. In Eq. (38), the summand $\langle k_{ij}^{(\mathrm{AA})}(\tau)\rangle_{x_{ij}}$ is shown to take different forms depending on the magnitude of x_{ij}, which should be considered in evaluating $\langle k^{(\mathrm{AA})}(\tau)\rangle_x$. In the plane of (i,j) with $j>i$ (Fig. 8), on which the summation in Eq. (40) is taken, the critical line $j=\tau_{c1}(i)$ with

$$\tau_{c1}(i)=\left(\frac{\tau_c x}{i}\right)^{\mu_A/\mu_A-1} i \tag{D2}$$

distinguishes the different behaviors of $\langle k_{ij}^{(\mathrm{AA})}(\tau)\rangle_{x_{ij}}$; $\langle k_{ij}^{(\mathrm{AA})}(\tau)\rangle_{x_{ij}}\simeq \ell_A(\tau_c x/j)(j/i)^{1/\mu_A}$ for $j\gg\tau_{c1}(i)$ and $\simeq\ell_A$ for $j\ll\tau_{c1}(i)$. The curve $j=\tau_{c1}(i)$ meets the line $j=\tau$ and $j=i$ at $i=\tau_{c2}$ and $i=\tau_{c3}$, respectively, with

$$\tau_{c2}=\tau\left(\frac{\tau_c x}{\tau}\right)^{\mu_A},\quad \tau_{c3}=\tau_c x. \tag{D3}$$

See Fig. 8. These characteristic values turn out to be useful in evaluating the function Φ as below.

In the case of $\frac{\tau_c x}{\tau}\gg 1$, it holds that $\tau_{c2}\gg\tau$ and thus $\langle k_{ij}^{(\mathrm{AA})}(\tau)\rangle_x\simeq\ell_A$ in the whole region $\{(i,j)|1\leqslant i\leqslant\tau, i<j\leqslant\tau\}$, leading to

$$\Phi\simeq\frac{1}{\ell_A}\frac{2}{\tau^2}\sum_{i=1}^{\tau}\sum_{j=i+1}^{\tau}\ell_A\simeq 1. \tag{D4}$$

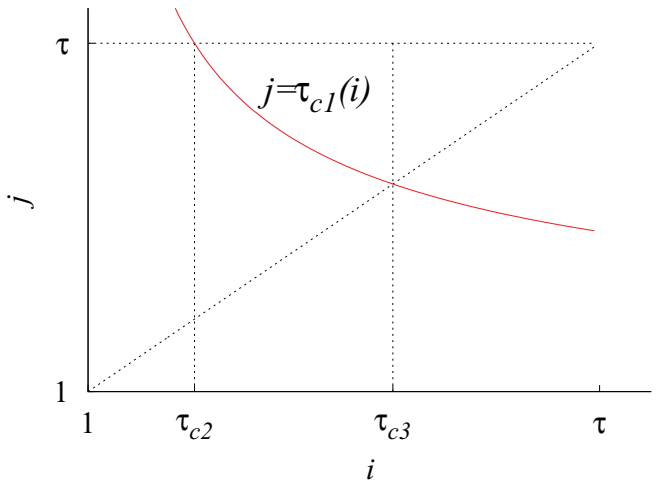

FIG. 8. (Color online) Characteristic curve τ_{c1} and values τ_{c2} and τ_{c3} in the (i,j) plane useful for the computation of Eq. (40).

In the case of $\tau^{-1/\mu_A}\ll\frac{\tau_c x}{\tau}\ll 1$, it holds that $1\ll\tau_{c2}\ll\tau_{c3}\ll\tau$ and therefore the functional form of $\langle k_{ij}^{(\mathrm{AA})}(\tau)\rangle_x$ varies with i and j. Assuming that $\langle k_{ij}^{(\mathrm{AA})}(\tau)\rangle_x\simeq\ell_A\frac{\tau_c x}{j}(\frac{j}{i})^{1/\mu_A}$ in the whole region of (i,j), one would obtain

$$\begin{aligned} \Phi_0 &\simeq \frac{1}{\ell_A}\frac{2}{\tau^2}\sum_{i=1}^{\tau}\sum_{j=i+1}^{\tau}\ell_A\frac{\tau_c x}{j}\left(\frac{j}{i}\right)^{1/\mu_A} \\ &\simeq \frac{2\tau_c x}{\tau^2}\sum_{i=1}^{\tau}\frac{1}{i^{1/\mu_A}}\frac{\tau^{1/\mu_A}-i^{1/\mu_A}}{\frac{1}{\mu_A}} \\ &\simeq \frac{2\tau_c x\mu_A}{\tau^2}\left[\tau^{1/\mu_A}\left\{\frac{\tau^{1-1/\mu_A}-1}{1-\frac{1}{\mu_A}}\right\}-\tau+1\right] \\ &\simeq \frac{2\mu_A}{\mu_A-1}\frac{\tau_c x}{\tau}. \end{aligned} \tag{D5}$$

The function Φ is then represented as

$$\Phi=\Phi_0-C \tag{D6}$$

with the function C evaluated as

$$\begin{aligned} C &\simeq \frac{2}{\tau^2}\left(\sum_{i=1}^{\tau_{c2}}\sum_{j=i+1}^{\tau}+\sum_{i=\tau_{c2}}^{\tau_{c3}}\sum_{j=i+1}^{\tau_{c1}(i)}\right)\left(\frac{\tau_c x}{j}\left(\frac{j}{i}\right)^{\frac{1}{\mu_A}}-1\right) \\ &\simeq \frac{2}{\tau^2}\sum_{i=1}^{\tau_{c2}}\left(\frac{\tau_c x}{i^{\frac{1}{\mu_A}}}\frac{\tau^{\frac{1}{\mu_A}}-i^{\frac{1}{\mu_A}}}{\frac{1}{\mu_A}}-\tau+i\right)+\frac{2}{\tau^2}\sum_{i=\tau_{c2}}^{\tau_{c3}}\left\{\frac{\tau_c x}{i^{\frac{1}{\mu_A}}}\frac{\left(\frac{\tau_c x}{i}\right)^{\frac{1}{\mu_A-1}}i^{\frac{1}{\mu_A}}-i^{\frac{1}{\mu_A}}}{\frac{1}{\mu_A}}-\left(\frac{\tau_c x}{i}\right)^{\frac{\mu_A}{\mu_A-1}}i+i\right\} \\ &\simeq \frac{2}{\tau^2}\left\{\mu_A\tau_c x\frac{\tau\left(\frac{\tau_c x}{\tau}\right)^{\mu_A-1}}{1-\frac{1}{\mu_A}}-\tau^2\left(\frac{\tau_c x}{\tau}\right)^{\mu_A}+\mu_A\tau_c x\left(\frac{\tau\left(\frac{\tau_c x}{\tau}\right)-\tau\left(\frac{\tau_c x}{\tau}\right)^{\mu_A-1}}{1-\frac{1}{\mu_A-1}}-\tau\left(\frac{\tau_c x}{\tau}\right)\right)\right. \\ &\quad\left.-\frac{\tau^2\left(\frac{\tau_c x}{\tau}\right)^2-\tau^2\left(\frac{\tau_c x}{\tau}\right)^{\mu_A}}{1-\frac{1}{\mu_A-1}}+\frac{1}{2}\tau^2\left(\frac{\tau_c x}{\tau}\right)^2\right\} \\ &\simeq \frac{2}{(\mu_A-1)(2-\mu_A)}\left(\frac{\tau_c x}{\tau}\right)^{\mu_A}+\frac{\mu_A}{\mu_A-2}\left(\frac{\tau_c x}{\tau}\right)^2. \end{aligned} \tag{D7}$$

In the considered case, $\tau_c x/\tau \ll 1$, the small-z behavior of $\Phi(z)$ with $z = \tau_c x/\tau$ is of interest, which is given by

$$\Phi(z) \simeq 2\frac{\mu_A}{\mu_A - 1} - \begin{cases} \frac{2}{(\mu_A-1)(2-\mu_A)} \left(\frac{\tau_c x}{\tau}\right)^{\mu_A} & \text{for} \quad \mu_A < 2, \\ \frac{\mu_A}{\mu_A-2} \left(\frac{\tau_c x}{\tau}\right)^2 & \text{for} \quad \mu_A > 2. \end{cases} \tag{D8}$$

[1] R. Albert and A.-L. Barabási, Rev. Mod. Phys. **74**, 47 (2002).
[2] M. Pascual and J. Dunne, *Ecological Networks: Linking Structure to Dynamics in FoodWebs* (Oxford University Press, New York, 2005).
[3] See http://www.nceas.ucsb.edu/interactionweb/resources.html
[4] E. Thébault and C. Fontaine, Science **329**, 853 (2010).
[5] J. Bascompte, P. Jordano, C. J. Melian, and J. M. Olesen, Proc. Natl. Acad. Sci. USA **100**, 9383 (2003).
[6] M. Kurant and P. Thiran, Phys. Rev. Lett. **96**, 138701 (2006).
[7] S. V. Buldyrev, R. Parshani, G. Paul, H. E. Stanley, and S. Havlin, Nature (London) **464**, 1025 (2010).
[8] P. J. Mucha, T. Richardson, K. Macon, M. A. Porter, and J.-P. Onnela, Science **328**, 876 (2010).
[9] R. Parshani, S. V. Buldyrev, and S. Havlin, Phys. Rev. Lett. **105**, 048701 (2010).
[10] R. Parshani, S. V. Buldyrev, and S. Havlin, Proc. Natl. Acad. Sci. USA **108**, 1007 (2011).
[11] J. Gao, S. V. Buldyrev, S. Havlin, and H. E. Stanley, Phys. Rev. Lett. **107**, 195701 (2011).
[12] C. D. Brummitt, R. M. D'Souza, and E. Leicht, Proc. Natl. Acad. Sci. USA **109**, E680 (2012).
[13] P. Jordano, J. Bascompte, and J. M. Olesen, Ecol. Lett. **6**, 69 (2003).
[14] P. R. Guimarães, Jr., G. Machado, M. A. de Aguiar, P. Jordano, J. Bascompte, A. Pinheiro, and S. F. dos Reis, J. Theor. Biol. **249**, 181 (2007).
[15] K. Takemoto and M. Arita, J. Theor. Biol. **264**, 782 (2010).
[16] D. P. Vázquez, Oikos **108**, 421 (2005).
[17] L. Santamaría and M. A. Rodríguez-Gironés, PLoS Biol. **5**, e31 (2007).
[18] S. Saavedra, F. Reed-Tsochas, and B. Uzzi, Nature (London) **457**, 463 (2009).
[19] C. Campbell, S. Yang, R. Albert, and K. Shea, Proc. Natl. Acad. Sci. USA **108**, 197 (2011).
[20] R. J. Williams, PLoS ONE **6**, e17645 (2011).
[21] M. M. Pires, P. I. Prado, and P. R. Guimarães, Jr., PloS One **6**, e27280 (2011).
[22] L. N. Joppa and R. Williams, PLoS ONE **8**, e56277 (2013).
[23] S. E. Maeng, J. W. Lee, and D.-S. Lee, Phys. Rev. Lett. **108**, 108701 (2012).
[24] B. Hughes, *Random Walks and Random Environments* (Clarendon Press, Oxford, 1995).
[25] J. Cárdenas, M. Mourounte, R. Benito, and J. Losada, Physica A **389**, 1789 (2010).
[26] A.-L. Barabási and R. Albert, Science **286**, 509 (1999).
[27] J. Wuttke, Algorithms **5**, 604 (2012).
[28] E. W. Montroll and J. T. Bendler, J. Stat. Phys. **34**, 129 (1984).
[29] E. Gumbel, *Statistics of Extremes* (Columbia University Press, New York, 1958).
[30] D.-S. Lee, K.-I. Goh, B. Kahng, and D. Kim, Nucl. Phys. B **696**, 351 (2004).
[31] E. Ravasz, A. Somera, D. Mongru, Z. Oltvai, and A.-L. Barabási, Science **297**, 1551 (2002).
[32] M. Almeida-Neto, P. R. Guimarães, Jr., R. D. Loyola, and W. Ulrich, Oikos **117**, 1227 (2008).
[33] U. Bastolla, M. A. Fortuna, A. Pascual-García, A. Ferrera, B. Luque, and J. Bascompte, Nature (London) **458**, 1018 (2009).